

# Biomedical Application of Non-Thermal Atmospheric Pressure Plasma and Its Usefulness

Guest Editor: Tetsuo Adachi

## Gas-liquid interfacial plasmas producing reactive species for cell membrane permeabilization

Toshiro Kaneko,<sup>1,\*</sup> Shota Sasaki,<sup>1</sup> Keisuke Takashima<sup>1</sup> and Makoto Kanzaki<sup>2</sup>

<sup>1</sup>Department of Electronic Engineering and <sup>2</sup>Department of Biomedical Engineering, Tohoku University, 6-6-05 Aoba, Aramaki, Aoba-ku, Sendai 980-8579, Japan

(Received 14 August, 2016; Accepted 17 September, 2016; Published online 17 December, 2016)

**Gas-liquid interfacial atmospheric-pressure plasma jets (GLI-APPJ) are used medically for plasma-induced cell-membrane permeabilization. In an attempt to identify the dominant factors induced by GLI-APPJ responsible for enhancing cell-membrane permeability, the concentration and distribution of plasma-produced reactive species in the gas and liquid phase regions are measured. These reactive species are classified in terms of their life-span: long-lived (e.g., H<sub>2</sub>O<sub>2</sub>), short-lived (e.g., O<sub>2</sub><sup>•-</sup>), and extremely-short-lived (e.g., •OH). The concentration of plasma-produced •OH<sub>aq</sub> in the liquid phase region decreases with an increase in solution thickness (<1 mm), and plasma-induced cell-membrane permeabilization is found to decay markedly as the thickness of the solution increases. Furthermore, the horizontally center-localized distribution of •OH<sub>aq</sub> resulting from the center-peaked distribution of •OH in the gas phase region, corresponds with the distribution of the permeabilized cells upon APPJ irradiation, whereas the overall plasma-produced oxidizing species such as H<sub>2</sub>O<sub>2aq</sub> in solution exhibit a doughnut-shaped horizontal distribution. These results suggest that •OH<sub>aq</sub> is likely one of the dominant factors responsible for plasma-induced cell-membrane permeabilization.**

**Key Words:** gas-liquid interfacial plasma, atmospheric-pressure plasma jet, plasma medicine, reactive species, cell membrane permeabilization

Non-equilibrium atmospheric-pressure plasmas (APPs) in a liquid or in contact with a liquid are called gas-liquid interfacial atmospheric-pressure plasmas (GLI-APPs).<sup>(1,2)</sup> GLI-APPs have attracted much attention as a novel technology that provides new physical<sup>(3)</sup> and chemical<sup>(4,5)</sup> effects on the surface of the liquid, resulting in the likelihood of exotic reactions in the liquid. Several applications of GLI-APPs have been developed in materials science including nanoparticle synthesis,<sup>(6,7)</sup> surface treatment of nanomaterials,<sup>(8)</sup> and the decomposition of persistent substances,<sup>(9)</sup> as well as life science applications in medicine,<sup>(10–12)</sup> agriculture<sup>(13,14)</sup> and biology.<sup>(15)</sup>

There are two types of GLI-APPs.<sup>(16)</sup> In one type, the discharge plasma is generated using a liquid electrode: the APP is generated between a powered electrode in the gas phase region and a grounded electrode in the liquid phase region, namely the liquid works as the electrode.<sup>(4,5)</sup> Liquid-electrode plasmas include in-liquid plasmas, where the powered electrode is also immersed in the liquid phase region. The plasma is mainly generated in gas bubbles formed in the liquid using an arc,<sup>(17)</sup> streamer,<sup>(18)</sup> pulsed

direct current (DC) glow,<sup>(19)</sup> or microwave discharge<sup>(20,21)</sup> immersed in a liquid, such as water,<sup>(22)</sup> organic solvent,<sup>(23)</sup> liquid nitrogen<sup>(24)</sup> or supercritical carbon dioxide.<sup>(25)</sup>

In the other type of GLI-APPs, the discharge plasma is generated between metal electrodes in the gas phase region, and then irradiated onto the liquid. One example is the atmospheric pressure plasma jet (APPJ),<sup>(26,27)</sup> which is widely used for applications in both materials and life sciences because it is easy to generate and can be used to gently irradiate various kinds of materials. Irradiating liquids with the APPJ (GLI-APPJ) conduces to a large number of reactions caused by plasma-induced stimuli, such as electric fields, ultraviolet (UV) light, reactive species, temperature and shock waves (Fig. 1).<sup>(26)</sup> Many studies on applications of GLI-APPJ to plasma medicine have reported exciting results using the plasma-induced stimuli, including the selective killing of cancer cells,<sup>(28–30)</sup> blood coagulation for minimally invasive surgery,<sup>(31,32)</sup> wound healing and tissue regeneration,<sup>(33–35)</sup> and cell membrane permeabilization.<sup>(36–42)</sup>

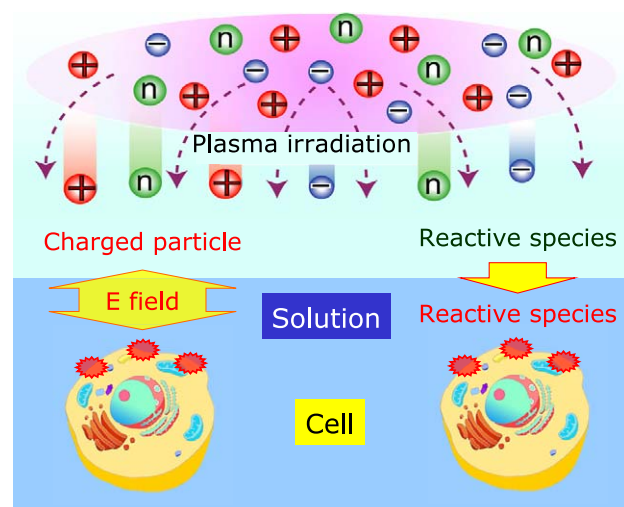


Fig. 1. Effects of gas-liquid interfacial plasmas on cell activities.

\*To whom correspondence should be addressed.  
E-mail: kaneko@ecei.tohoku.ac.jp

Given previous reports that hydroxyl radical ( $\cdot\text{OH}$ ) plays an important role in mediating the biological effects of plasma<sup>(43,44)</sup> and that it is produced in both the gas and liquid phase regions, in this paper we focus on  $\cdot\text{OH}$  produced by GLI-APPJ and investigate its effect on cell-membrane permeability.

### Atmospheric Pressure Plasma Jet in Contact with Liquid

Researchers in the plasma life science field make and use various kinds of APPJs that differ in electrode configuration, excitation frequency (pulsed DC,<sup>(45)</sup> LF ( $\sim\text{kHz}$ ),<sup>(46)</sup> RF ( $\sim\text{MHz}$ ),<sup>(47,48)</sup> microwaves ( $\sim\text{GHz}$ )<sup>(49)</sup> and working gas (He, Ar, O<sub>2</sub>, N<sub>2</sub>, H<sub>2</sub>O). The choice of electrode, frequency, and working gas dictates the electron density and temperature, and the gas temperature of the generated plasma in the gas phase region, resulting in changes in the density of the excited particles such as metastable He\* and Ar\*, and various kinds of reactive species such as  $\cdot\text{OH}$ , H<sub>2</sub>O<sub>2</sub>, HO<sub>2</sub> and NO<sub>x</sub>.

When these excited particles and reactive species in the gas phase region contact liquid, other reactive species are produced at the interface between the plasma and liquid. These newly-produced reactive species in the liquid phase region likely affect the activity of cells in the liquid, but these reactive species have a limited life-span and gradually disappear with time. Therefore, the distance between the plasma-liquid interface and a cell is important for effective control of cell activity. Consequently, to clarify the behavior of the reactive species produced by the GLI-APPJ, the reactive species should be measured in both the gas and liquid phase regions, and the temporal and spatial distributions of the reactive species should also be analyzed.

A schematic illustration of a typical experimental setup for investigating the effects of reactive species produced by the GLI-APPJ on cell activities<sup>(41)</sup> is shown in Fig. 2A. The APPJ apparatus consists of a quartz tube (6-mm inner diameter and 10-mm outer diameter) with two electrodes. The powered electrode is a 1.5-mm diameter tungsten rod, and the grounded electrode is an aluminum foil on the outer surface of the quartz tube. He gas is used as the source gas and its flow rate ( $f$ ) through the dielectric tube is regulated by a mass flow controller (MFC). Turning on the high-voltage ( $V_{p-p}$ ) power supply (which has a frequency of 8–10 kHz)

generates He-APP that flows from the nozzle of a glass tube (2-mm inner diameter), irradiating the cell-suspended solution in chamber slides kept on a hot plate (37°C). The parameter  $L_{dif}$  is defined as the distance between the bottom edge of the powered electrode and the surface of the solution in the chamber slides. Typical conditions of operation are  $V_{p-p} = 5\text{--}10\text{ kV}$ ,  $f = 1\text{--}3\text{ L/min}$ , and  $L_{dif} = 45\text{--}60\text{ mm}$ .

### Reactive Species in the Gas Phase Region

Strong emission of visible He-APP is observed between the powered electrode and the surface of the solution (Fig. 2B) and the strength of the emission, i.e., the plasma density, can be changed by controlling the distance  $L_{dif}$ .<sup>(41)</sup> The distance between the surface of the solution and the discharge electrode significantly influences various physical and chemical characteristics such as plasma length, shape, color, voltage, current, and the composition of the plasma-produced reactive species.<sup>(50–52)</sup>

The current apparatus uses only He as the source gas to generate the APP, yet various reactive oxygen and nitrogen species (RONS) are produced in the gas phase region because ambient air is mixed in the He-APP. The density of RONS in the He-APP (gas phase region) has been evaluated using several measurement methods such as optical emission spectroscopy (OES),<sup>(53,54)</sup> Fourier transform infrared spectroscopy (FT-IR),<sup>(55)</sup> and laser-induced fluorescence (LIF).<sup>(56,57)</sup> Here, we focus on OH radicals as a typical reactive species and use  $\cdot\text{OH}$  laser-induced fluorescence (OH-LIF)<sup>(58,59)</sup> to measure the density and temperature of the plasma-produced  $\cdot\text{OH}$  in the APPJ with high spatial resolution. A wavelength-tunable dye laser outputs a 566 nm beam diameter of 4 mm whose frequency doubled beam corresponding with  $\cdot\text{OH}$ (A-X) transition at 283 nm. The 283 nm UV beam is shaped into a 1 mm  $\times$  11 mm beam sheet using lenses after beam energy tuning with a polarizing beam splitter and a half wave plate. The typical operational beam energy is up to 0.5 mJ/pulse and the estimated mean beam intensity is approximately  $1 \times 10^5\text{ W/cm}^2$ . An ICCD camera is used to collect the  $\cdot\text{OH}$  fluorescence through a UV camera lens, and a narrow band pass filter centered at 309.5 nm with a full width at half maximum (FWHM) of 9 nm is used to obtain the two-dimensional distribution of  $\cdot\text{OH}$  fluorescence in the

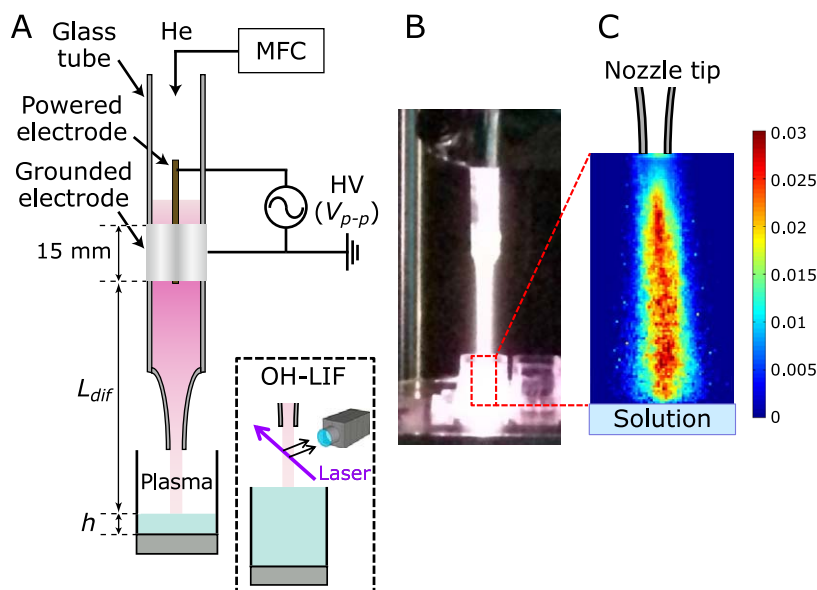


**Fig. 2.** (A) Schematic illustration of the experimental setup for investigating the membrane permeability of adherent cells exposed to APPJ and the two-dimensional distribution of OH radicals in the gas phase using the LIF technique. (B) Typical photographs of APPJ irradiation and (C) two-dimensional distribution of OH radicals in the gas phase region.

gas phase region. The  $\cdot\text{OH}$  fluorescence images are normalized by Rayleigh scattering and corrected for fluorescence yield and Boltzmann factor with measured quenching rate of  $\cdot\text{OH}$  and two rotational lines of  $P_1(2)$  and  $Q_1(5)$ , thus Fig. 2C indicates two-dimensional  $\cdot\text{OH}$  density distribution. In the horizontal direction, the density of  $\cdot\text{OH}$  has a peak at the geometrical axis. In the axial direction, the  $\cdot\text{OH}$  density remains high especially near the nozzle exit and in the vicinity of the solution surface, which shows that  $\cdot\text{OH}$  does not decay along with helium flow (11 mm from the exit). Therefore, the GLI-APPJ can supply a large amount of  $\cdot\text{OH}$  in solution and the maximum distribution of  $\cdot\text{OH}$  is in the center of the gas phase region.

### Reactive Species in the Liquid Phase Region

The reactive species produced in the gas phase region are irradiated onto the liquid phase region, thus generating new reactive species. These new reactive species react with each other depending on their respective reaction rate<sup>(60)</sup> and change into other chemical species within a certain time scale, which we define as life-span. We classify the reactive species based on their life-span into long-lived (life-span on the order of hours or more), short-lived (life-span on the order of minutes), or extremely-short-lived (life-span on the order of seconds or less). Long-lived reactive species can be measured by ion chromatography and optical absorption of the plasma irradiated solution,<sup>(61,62)</sup> whereas short-lived and extremely-short-lived reactive species are measured primarily using the chemical probe method, where the short-lived species react with specific chemicals and are changed into relatively long-lived chemical species which are then analyzed by techniques such as photoluminescence<sup>(63,64)</sup> and electron spin resonance (ESR).<sup>(65–67)</sup>

**Long-lived reactive species.** The long-lived reactive species in the plasma irradiated solution are analyzed by an optical absorption method (Fig. 3A). The absorbance spectrum of the plasma irradiated buffer solution (5 mM  $\text{NaHCO}_{3\text{aq}}$ ) between 230 and 300 nm is fitted with synthesized spectra generated by linear combination of the absorption spectra of  $\text{H}_2\text{O}_{2\text{aq}}$ ,  $\text{NO}_3^-\text{aq}$ , and  $\text{NO}_2^-\text{aq}$  (Fig. 3B). The concentrations of these reactive species produced in the plasma irradiated solution are estimated from the least-square-error fitting of the synthetic spectrum to the measured absorption spectrum (Fig. 3C). The error bars plotted in Fig. 3C are the 99% confidence intervals of the fitting coefficients in the synthetic spectrum. The estimated concentrations of the reactive species are obtained as a function of the plasma irradiation time  $t_i$ .

**Short-lived reactive species.** The chemical probe method is used to observe the existence of short-lived and extremely-short-lived reactive species in the liquid phase region (Fig. 4A).

The total production of OH radicals as extremely-short-lived reactive species in the liquid phase ( $\cdot\text{OH}_{\text{aq}}$ ) after plasma irradiation is detected using terephthalic acid (TA).<sup>(63,64)</sup> Plasma-produced  $\cdot\text{OH}_{\text{aq}}$  can convert terephthalate anion (produced from TA) to 2-hydroxyterephthalate ion (HTA), a highly fluorescent material. HTA is optically excited by 310-nm UV light and emits strong fluorescence around 425 nm. The total production of  $\cdot\text{OH}_{\text{aq}}$  can be estimated from the fluorescence intensity due to the linear relationship between the fluorescence intensity around 425 nm and the concentration of HTA ( $C_{\text{HTA}}$ ). A solution of 2 mM TA was prepared, warmed to 37°C, and exposed to APPJ for  $t_i$ , then the fluorescence of the solution was measured.  $C_{\text{HTA}}$  is analyzed as a function of  $t_i$  (Fig. 4B); the inset shows the fluorescence spectra of HTA solution after APPJ irradiation for different  $t_i$ .  $C_{\text{HTA}}$ , an indicator of total  $\cdot\text{OH}_{\text{aq}}$  production, increased linearly with increasing  $t_i$ .

**Spatial distribution of short-lived reactive species.** HTA generated from TA by  $\cdot\text{OH}_{\text{aq}}$  is observed throughout the solution region, but actually  $\cdot\text{OH}_{\text{aq}}$  is produced and exists primarily at the surface of the plasma-irradiated solution; this is especially the case for extremely-short-lived reactive species such as  $\cdot\text{OH}_{\text{aq}}$ . To evaluate the amount of extremely-short-lived reactive species produced at the plasma-liquid interface can reach the bottom of the solution, which is where the living cells in the sample are located, we measure the distribution of the short-lived reactive species at the bottom of the chamber slides for different solution thicknesses.

A gel reagent containing TA is used to measure the distribution of plasma-produced  $\cdot\text{OH}_{\text{aq}}$  (Fig. 5A). This gel reagent is a modification of a potassium iodide (KI)-starch gel reagent based on the well-known iodine-starch reaction<sup>(68,69)</sup> typically used to measure the two-dimensional concentration distribution of reactive oxygen species. Photographs (6 mm × 6 mm area) of the gel reagent after plasma irradiation for  $t_i = 5$  s are shown in Fig. 5B. Fluorescence profiles along the X-axis are obtained for solution thickness  $h = 0.5, 0.7,$  and  $1.0$  mm (Fig. 5C). The fluorescence of the gel reagent reflects the concentration of  $\cdot\text{OH}_{\text{aq}}$  and its vertical distribution decreases with increasing solution thickness.<sup>(41)</sup> Therefore, a relatively large amount of  $\cdot\text{OH}_{\text{aq}}$  is produced at the surface of the solution, but the  $\cdot\text{OH}_{\text{aq}}$  immediately disappear through the solution within 1 mm.

Short-lived reactive species other than  $\cdot\text{OH}$ , including various reactive oxygen and nitrogen species, are produced in plasma-irradiated solutions and behave as reactive chemical oxidants.<sup>(43)</sup> The distributions of plasma-produced oxidizing species in solution are detected using a gel reagent containing KI-starch, as mentioned above. A 0.5% agarose/water solution containing 0.3% potassium iodide and 0.5% starch is prepared and then gels in the

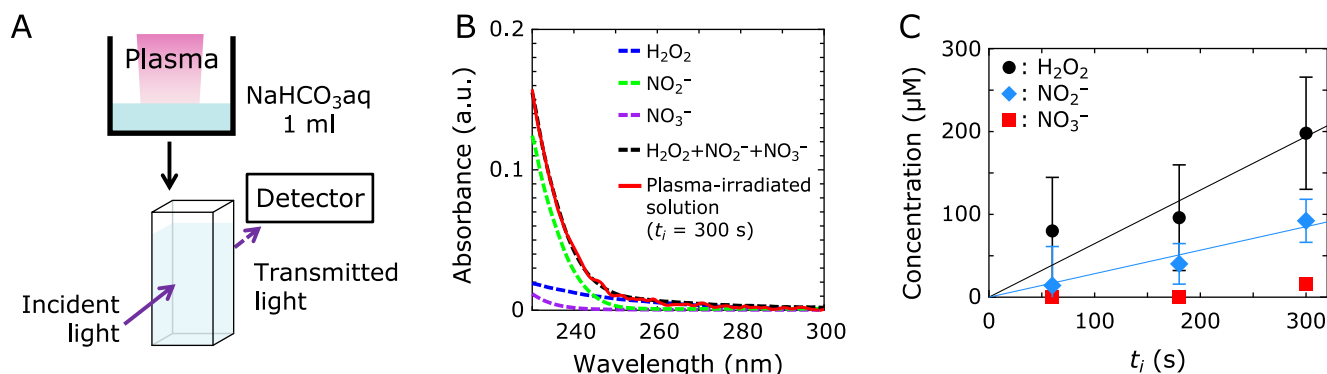


**Fig. 3.** (A) Schematic illustration of the experimental setup for measuring UV absorption spectra to obtain the concentration of the reactive species. (B) UV absorption spectra of  $\text{NO}_{2\text{aq}}$ ,  $\text{NO}_{3\text{aq}}$ , and  $\text{H}_2\text{O}_{2\text{aq}}$  and the plasma-irradiated solution. (C) Concentration of  $\text{NO}_{2\text{aq}}$ ,  $\text{NO}_{3\text{aq}}$ , and  $\text{H}_2\text{O}_{2\text{aq}}$  as a function of the plasma irradiation time  $t_i$ .

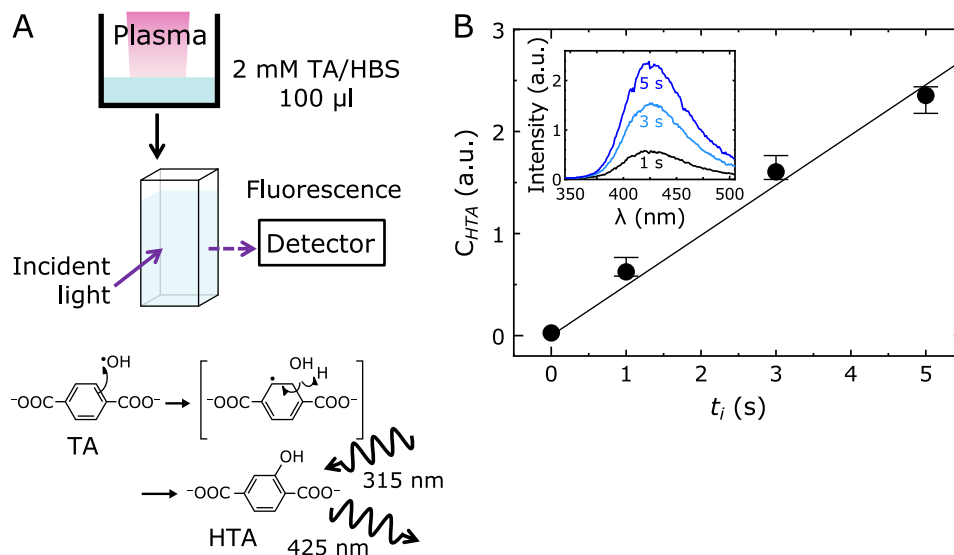


**Fig. 4.** (A) Schematic illustration of the experimental setup for measuring fluorescence of HTA solution and (B) the concentration of HTA ( $C_{HTA}$ ), an indicator of total  $\cdot\text{OH}_{\text{aq}}$  production, as a function of plasma irradiation time  $t_i$ . The inset shows fluorescence spectra of HTA solution after APPJ irradiation for different  $t_i$ .

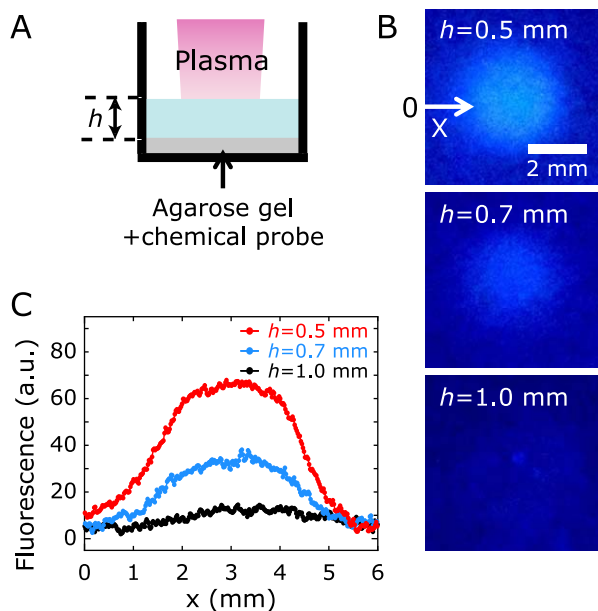


**Fig. 5.** (A) Schematic illustration of the experimental setup for measuring the horizontal distribution of plasma-produced  $\cdot\text{OH}_{\text{aq}}$  using a gel reagent containing TA. (B) Photographs ( $6\text{ mm} \times 6\text{ mm}$  area) of the gel reagent (TA) after plasma irradiation for  $t_i = 5\text{ s}$ , and (C) fluorescence profiles along the X-axis for solution thickness  $h = 0.5, 0.7,$  and  $1.0\text{ mm}$ .

chamber slide. The solution is poured onto the gel reagent at room temperature with its thickness ( $h$ ) controlled and then exposed to APPJ for  $t_i$ . The obtained image of the gel reagent is then analyzed.

Photographs ( $6\text{ mm} \times 6\text{ mm}$  area) of the gel reagent after plasma irradiation for  $t_i = 5\text{ s}$  are shown in Fig. 6A. The absorbance profiles along the X-axis are obtained for solution thickness  $h = 0.5, 0.7$  and  $1.0\text{ mm}$  (Fig. 6B). The absorbance of the gel reagent indicates the concentration of the oxidizing reactive species and its vertical distribution decreases with increasing solution thickness. In addition, the oxidizing reactive species are

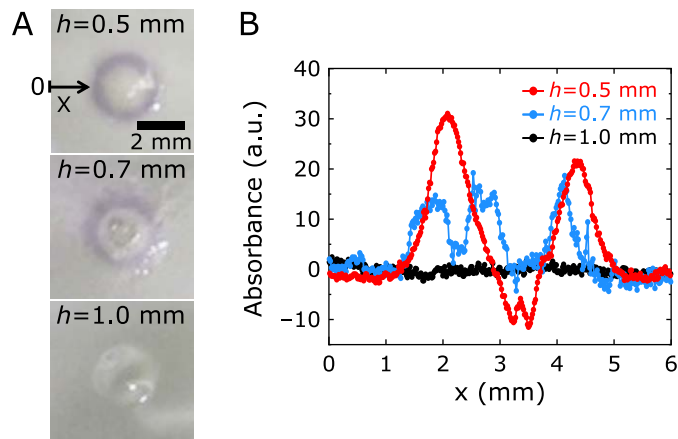


**Fig. 6.** (A) Photographs ( $6\text{ mm} \times 6\text{ mm}$  area) of the gel reagent (KI-Starch) after plasma irradiation for  $t_i = 5\text{ s}$ , and (B) absorbance profiles along the X-axis for solution thickness  $h = 0.5, 0.7,$  and  $1.0\text{ mm}$ .

found to be horizontally distributed in a doughnut shape,<sup>(41)</sup> as previously reported by Kawasaki *et al.*<sup>(68,69)</sup> However, as shown in Fig. 5B and C, the horizontal distribution of  $\cdot\text{OH}_{\text{aq}}$  is not doughnut shaped and clearly differs from that of other oxidizing species. Based on these results,  $\cdot\text{OH}_{\text{aq}}$  in the liquid phase region is produced mainly in the central region of the plasma-solution interface, and this corresponds to the distribution of  $\cdot\text{OH}$  in the gas phase region. In contrast, the predominant oxidizing species in solution detected in a doughnut-shaped distribution could be produced by reactive species other than  $\cdot\text{OH}$  and these reactive species are generated upon mixing ambient air in the gas phase region of the He-APP.

### Cell Membrane Permeabilization by Gas-Liquid Interfacial Atmospheric Pressure Plasmas

Cell membrane permeabilization is an important technique in molecular biology and medical procedures such as cancer pharmacotherapy,<sup>(70)</sup> gene therapy,<sup>(71)</sup> RNA-mediated suppression of gene

expression,<sup>(72)</sup> and the creation of induced pluripotent stem (iPS) cells.<sup>(73)</sup> However, electroporation,<sup>(74)</sup> a conventional method for permeabilizing cells, is problematic in terms of the low survival fraction, which reduces the efficacy of minimally invasive *in vivo* treatments. Recently, it was reported that genes can be efficiently introduced into cells using APP and that the method enables spatially selective membrane permeabilization.<sup>(36–38)</sup> Furthermore, the use of fluorescent dyes such as YOYO-1 and LIVE/DEAD Stain indicated that APP irradiation enhances the permeability of the cell membrane without killing the cell.<sup>(39–42)</sup> To understand the underlying mechanism of cell membrane permeabilization, we have investigated the effects of plasma-produced reactive species in the liquid phase region on cell activity. These plasma-produced reactive species reportedly play key roles in many medical applications of GLI-APPJ. We also investigated the relationship between plasma-induced cell membrane permeabilization and the spatial distributions of reactive species in the liquid phase region.

In this experiment, we use the non-membrane-permeative fluorescent dye YOYO-1 (Y3601, Molecular Probes) as the delivery material to investigate the effect of plasma irradiation on cell membrane permeability. The green fluorescence of YOYO-1 increases 1,000-fold when the dye is transferred into cells and binds double-stranded DNA (dsDNA) in the nucleus, allowing transfected cells to be easily identified.<sup>(75,76)</sup> In addition, YOYO-1 exhibits strong fluorescence within 0.5 s of binding to dsDNA, enabling rapid analysis of the fluorescence intensity of the cells and enumeration of the transfected cells as soon as the sample is irradiated with plasma.

Two types of plasma irradiation systems were fabricated to identify the reactive species produced by GLI-APPJ predominantly responsible for enhancing cell membrane permeability. One is a direct plasma irradiation (DPI) system (Fig. 7A), where a 100- $\mu$ l sample of solution containing floating cells and YOYO-1 is directly irradiated with APPJ for a specified irradiation time ( $t_i$ ). The other is an indirect plasma irradiation (IPI) system (Fig. 7B), where a 50- $\mu$ l sample of solution containing 10  $\mu$ M YOYO-1 is irradiated with plasma for a specified irradiation time  $t_i$ ; this plasma-irradiated solution is placed on ice for a defined period of time called the retention time  $t_r$ , then dripped into 50  $\mu$ l of solution containing floating cells ( $6 \times 10^6$  cells/ml). In each case, the cell solution is subsequently incubated on ice for 15 min. LIVE/DEAD Stain (L10120, Molecular Probes), a cell viability assay reagent, is dripped into the cell solution, which is then incubated at room temperature for 20 min and observed through a confocal laser scanning microscope. Because YOYO-1 (green) and LIVE/DEAD (red) stain emit different fluorescence wavelengths, we could observe their respective fluorescence signals using optical filters.

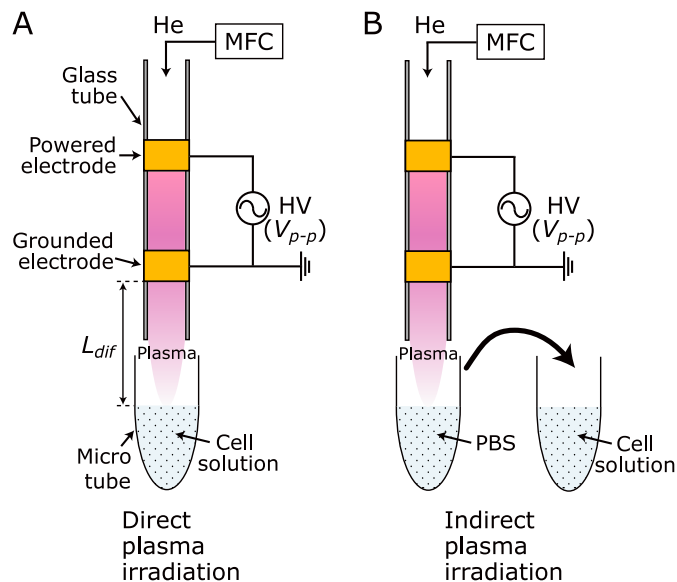


**Fig. 7.** Schematic illustration of the two types of plasma irradiation systems. (A) Direct plasma irradiation (DPI) and (B) indirect plasma irradiation (IPI).

We define the transfection efficiency  $\eta$  as the ratio of the number of transfected surviving cells to the total number of cells counted in the bright-field image. Cell viability is defined simply as the ratio of the number of surviving cells to the total number of cells counted.

Most of the reactive species produced in the plasma-irradiated solution are assumed to be short-lived and to dissipate rapidly with time. To investigate the effects of these transiently produced short-lived reactive species on cell membrane permeabilization, we measure the transfection efficiency  $\eta$  (%) of YOYO-1 as a function of the retention time  $t_r$  at  $t_i = 5$  s under IPI. The effect of the plasma-irradiated solution on transfection efficiency (i.e., enhancement of membrane permeability) decreases with increasing  $t_r$  and finally becomes constant (Fig. 8A). The effect observed beyond 30 min is due to long-lived reactive species such as  $H_2O_2$ , whereas the effect observed within the first several minutes is due to short-lived reactive species. In addition, the difference in transfection efficiency between DPI and IPI is likely due to direct effects such as extremely-short-lived reactive

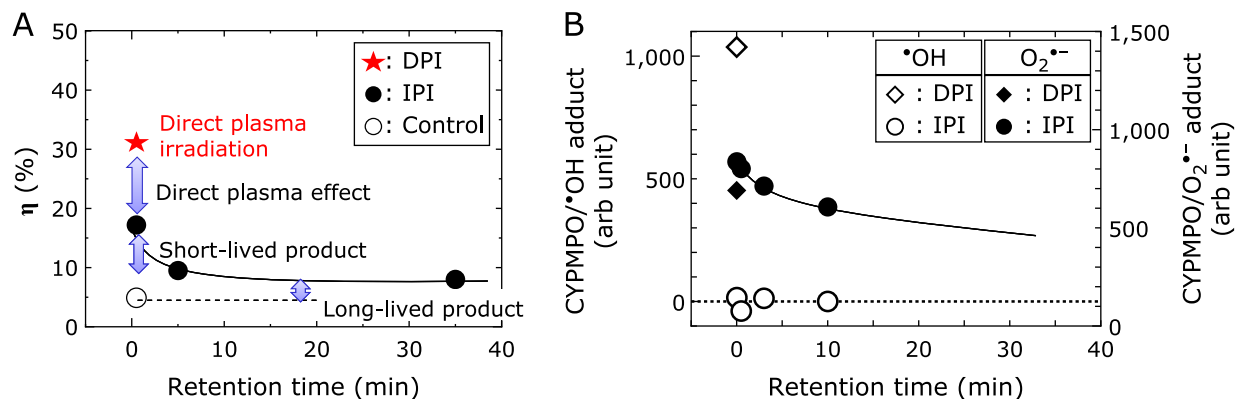


**Fig. 8.** (A) Transfection efficiency  $\eta$  (%) of YOYO-1 as a function of the retention time  $t_r$  at  $t_i = 5$  s under direct plasma irradiation (DPI) and indirect plasma irradiation (IPI). (B) Signal intensity of CYPMPO-OH (open diamond and circles) and CYPMPO-O<sub>2</sub><sup>-</sup> (filled diamond and circles) adducts as a function of the retention time  $t_r$  at  $t_i = 300$  s under DPI and IPI. Each plot was obtained in a single experiment.

species. Thus, factors that enhance cell membrane permeability can be classified as direct irradiation effects associated with extremely-short-lived species, and indirect irradiation effects due to short-lived and long-lived reactive species.

To identify these direct and indirect irradiation effects, we detect  $\cdot\text{OH}$  and superoxide anion radicals  $\text{O}_2^{\cdot-}$  in plasma-irradiated water using ESR.<sup>(65-67)</sup> The half-life of  $\text{O}_2^{\cdot-}$  is several tens of minutes in plasma-irradiated water at 4°C<sup>(42)</sup> and  $\text{O}_2^{\cdot-}$  is therefore a strong candidate as the short-lived key-product. The generation of  $\text{O}_2^{\cdot-}$  in water by APPJ irradiation is detected by ESR using 5-(2,2-dimethyl-1,3-propoxycyclophosphoryl)-5-methyl-1-pyrroline *N*-oxide (CYPMPO) as spin-trap because the reaction rate of CYPMPO with  $\text{O}_2^{\cdot-}$  is higher than that of the more commonly used 5,5-dimethyl *N*-oxide pyrroline (DMPO).<sup>(65)</sup> Moreover, the ESR spectra of CYPMPO-OH and CYPMPO- $\text{O}_2^{\cdot-}$  adducts are clearly separated and readily identifiable. For DPI experiments, 500- $\mu\text{l}$  of 5 mM CYPMPO/ultrapure water on ice is directly irradiated with plasma for  $t_i$ . For IPI experiments, 490- $\mu\text{l}$  of ultrapure water on ice is irradiated with plasma for  $t_i$ , put on ice for retention time  $t_r$ , and then dripped into 10- $\mu\text{l}$  of 250 mM CYPMPO/dimethyl sulfoxide (DMSO). In each case, ESR measurements are performed immediately after sample preparation.

The signal intensity of the ESR spectra of CYPMPO-OH (open diamond and circles) and CYPMPO- $\text{O}_2^{\cdot-}$  (filled diamond and circles) adducts are measured as a function of the retention time  $t_r$  at  $t_i = 300$  s under DPI or IPI (Fig. 8B). In the case of DPI, both CYPMPO-OH and CYPMPO- $\text{O}_2^{\cdot-}$  adducts are detected, whereas for IPI, CYPMPO-OH adducts derived from extremely-short-lived reactive species ( $\cdot\text{OH}$ ) are not detected but CYPMPO- $\text{O}_2^{\cdot-}$  adducts are detected for  $t_r = 1$  s. Moreover, the signal due to CYPMPO- $\text{O}_2^{\cdot-}$  adducts decreases with increasing  $t_r$ , indicating that the life-span of  $\text{O}_2^{\cdot-}$  in plasma-irradiated water on ice is of the order of minutes or longer.<sup>(42)</sup>

Taking account into the differences in the solutions used to obtain the results shown in Fig. 8A and B [Fig. 8A: PBS containing living cells and YOYO-1, Fig. 8B: water], the life-span of  $\text{O}_2^{\cdot-}$  in PBS containing living cells and YOYO-1 is expected to be shorter than that in water, making  $\text{O}_2^{\cdot-}$  a strong candidate as the short-lived reactive species that plays a critical role in IPI-induced cell membrane permeabilization. Furthermore, since CYPMPO-OH adducts are detected only in the case of DPI, the enhanced transfection efficiency observed using DPI is likely due to  $\cdot\text{OH}$  as the extremely-short-lived reactive species.

### Effects of Reactive Species Transport on Cell Membrane Permeabilization

Although the DPI method is effective for cell membrane permeabilization, it is difficult to understand the effects of the solution surrounding the floating cells because the distance between the cells and the surface of the solution, where the extremely-short-lived reactive species are produced, is uncontrolled. Therefore, we attempted to apply the DPI method to adherent cells instead of floating cells, where the distance between the adherent cells and the surface of the solution can be precisely controlled, thus allowing clarification of the effects on cell membrane permeability of the solution between the adherent cells and the plasma.

A typical DPI experiment ( $t_i = 2$  s,  $V_{p-p} = 5.9$  kV,  $h = 0.5$  mm) is shown in Fig. 9A. YOYO-1 fluorescence and bright field images of the cells after DPI in the peripheral region (no APPJ irradiation) are shown in Fig. 9B and in the central region (with APPJ irradiation) in Fig. 9C. YOYO-1 fluorescence is clearly observed in the central region but there is almost no fluorescence in the peripheral region. The estimated transfection efficiency in the APPJ irradiation area is more than 80%.

These results indicate that reactive species produced in the solution help the improvement in cell membrane permeability. If long-lived reactive species are produced in solution by the APPJ,

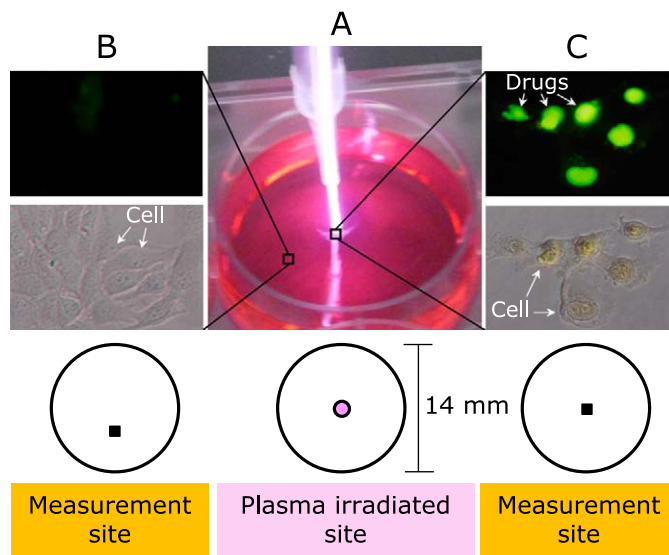


**Fig. 9.** (A) Typical pictures of GLI-APPJ irradiation in the central region. YOYO-1 fluorescence and bright field images of the cells after the GLI-APPJ irradiation (B) in the peripheral region (no APPJ irradiation) and (C) in the central region (with APPJ irradiation).

they may isotropically diffuse and the affected area should become larger. Since the transfection efficiency is increased only in the central region (the APP irradiation area), the improvement in cell membrane permeability results primarily from the extremely-short-lived reactive species, which are rapidly inactivated and thus cannot affect the cells in the peripheral region. These results indicate that cell activities are mainly enhanced by the transiently produced reactive species which have strong effects compared with long-lived reactive species such as  $\text{H}_2\text{O}_2$ .

The thickness of the solution layer ( $h$ ) is expected to affect cell membrane permeabilization due to the short life-span of the reactive species and thus we investigate the effects of the solution thickness (controlled by the volume of the solution added). A solution of 5  $\mu\text{M}$  YOYO-1/HEPES-buffered saline (HBS; containing 150 mM NaCl, 5 mM KCl, 2 mM  $\text{CaCl}_2$ , 1 mM  $\text{MgCl}_2$ , 5.6 mM D-glucose and 10 mM HEPES [pH adjusted to 7.4 with NaOH]) is prepared and kept at 37°C. The cell solution is exposed to APPJ for a plasma irradiation time  $t_i$  and is incubated at 37°C for 30 min, then fluorescence images of the cells are obtained using a fluorescence microscope (CKX41, Olympus). We calculate the integral of the number of pixels above a pre-determined threshold value of the fluorescence using ImageJ and define this value as an indicator of cell membrane permeabilization.

Fluorescence (YOYO-1) images after APPJ irradiation are observed with a solution layer of various thicknesses  $h$  (Fig. 10A). Plasma-induced cell membrane permeabilization is prominently observed as the solution layer thickness decreases and the transfer area increases in the horizontal direction. In addition, the amount of intracellular YOYO-1 (YOYO-1 transfer) is calculated as a function of  $h$  (Fig. 10B). These data show that YOYO-1 is transferred into cells over a larger area as the solution thickness decreases.<sup>(41)</sup>

As shown in Fig. 5B and C,  $\cdot\text{OH}_{\text{aq}}$  is widely distributed. The FWHM of a fluorescence peak from  $\cdot\text{OH}_{\text{aq}}$  is approximately 3 mm for  $h = 0.5$  mm, which drastically decreases as the solution thickness increases. At  $h = 0.5$  mm, YOYO-1 is transferred into cells over an area of approximately 3 mm in diameter but the transfer area decreases as the solution thickness increases. These data suggest that  $\cdot\text{OH}_{\text{aq}}$  may be the dominant factor in plasma-induced cell membrane permeabilization.

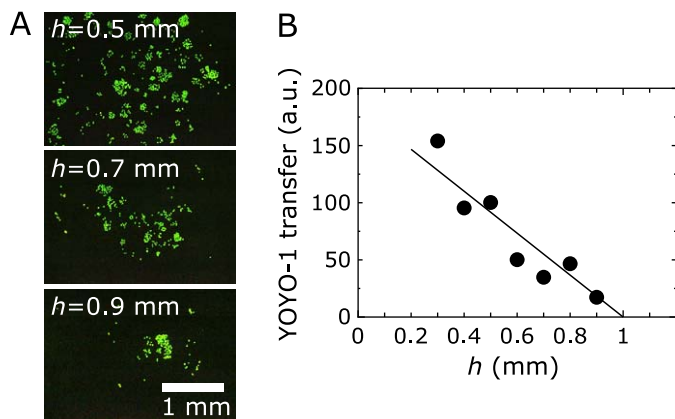


**Fig. 10.** (A) Fluorescence (YOYO-1) images after APPJ irradiation for solution thickness  $h = 0.5, 0.7,$  and  $0.9$  mm. (B) Amount of intracellular YOYO-1 (YOYO-1 transfer) as a function of solution thickness  $h$ .

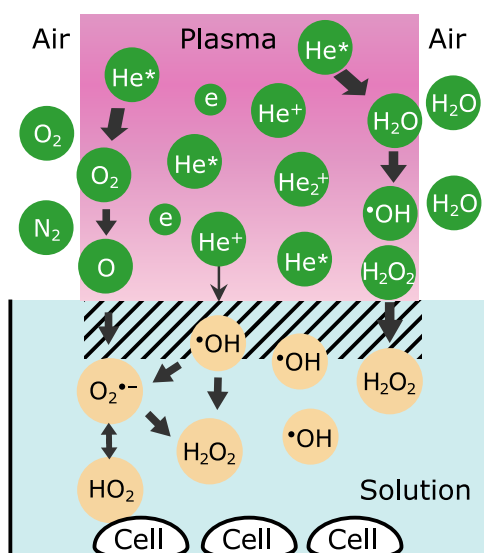


**Fig. 11.** Model of the reactive species transport from the gas phase region to the liquid phase region.

### Transport of Reactive Species from the Gas Phase to the Liquid Phase

The reactive species which affect cell activity are produced at the plasma-liquid interface. Computer simulations suggest that the reactive oxygen and nitrogen species in the gas phase region are produced by the diffusion of ambient air into excited-species rich He-APP including metastable helium  $He^*$  or air plasma, and the gas-phase OH radicals are mainly produced by the dissociation of  $H_2O$  near the plasma-liquid interface<sup>(77,78)</sup> (Fig. 11).

A relatively large amount of gas-phase OH is present along the central axis, where the He concentration is highest, and in the vicinity of the liquid surface, where the density of evaporated

water is highest. This suggests that  $\cdot OH$  production depends on metastable helium  $He^*$  and evaporated water. Since  $\cdot OH$  and other oxidizing species in the gas phase region are believed to be produced from evaporated water and oxygen in ambient air, the maximum concentration of  $\cdot OH_{aq}$  and oxidizing species in the liquid phase region is likely to be in the center and annular sections, respectively (Fig. 5 and 6). The concentration of plasma-produced  $\cdot OH_{aq}$  is higher in the center in the horizontal direction and decreases with solution thickness (Fig. 5), consistent with the distribution of YOYO-1 fluorescence, suggesting that  $\cdot OH_{aq}$  may be the dominant factor in plasma-induced cell membrane permeabilization.

$\cdot OH_{aq}$  is a precursor of other short- and long-lived reactive species, such as  $O_2^{\cdot -}$ ,  $H_2O_2$  and  $HNO_x$ <sup>(79,80)</sup> and these species can also alter the cell membrane structure.<sup>(81,82)</sup> Although the dominant factor in plasma-induced cell membrane permeabilization is likely to be  $\cdot OH_{aq}$  in the liquid phase region,  $\cdot OH_{aq}$  and other short-lived reactive species derived from  $\cdot OH_{aq}$  are candidates for causing the observed enhancement of cell membrane permeability.

These results provide insights that enhance our current understanding of the mechanism of cell membrane permeabilization by GLI-APPJ and could thus facilitate improvements in APPJ technology for cell membrane permeabilization (e.g., for introducing drugs or genes into cells).

### Conclusion

In summary, our aim was to identify the dominant factors in plasma-induced cell membrane permeabilization resulting from exposure to a gas-liquid interfacial atmospheric-pressure plasma jet (GLI-APPJ). We therefore observed the distribution of APPJ-produced reactive species in the gas and liquid phase regions, focusing primarily on OH radicals, and evaluated the effects of these reactive species on cell activity.

Plasma-produced  $\cdot OH_{aq}$  in the liquid phase region is distributed horizontally, with a higher concentration in the center resulting from the center-peaked  $\cdot OH$  distribution in the gas phase region. In contrast, the plasma-produced oxidizing species in solution are distributed horizontally in a doughnut shape, and most of these species are not  $\cdot OH_{aq}$ . Plasma-produced  $\cdot OH_{aq}$  decays and cell membrane permeabilization decreases in solution; the diffusion length of  $\cdot OH_{aq}$  is on the order of several hundred micrometers, suggesting that the production of  $\cdot OH_{aq}$  is a dominant factor in cell membrane permeabilization. However, not only  $\cdot OH_{aq}$  but also other short-lived and long-lived reactive species originating from  $\cdot OH_{aq}$  are candidates responsible for the observed enhancement of cell membrane permeability, as clarified by the indirect plasma irradiation experiment. A more detailed investigation of the effects of various plasma-produced reactive species on cell activity is required.

### Acknowledgments

This work was supported by JSPS KAKENHI Grant Nos. 24108004, 15K17480, and 15J01427. This work was also supported by the Knowledge-based Medical Device Cluster/Miyagi Area and by the Frontier Research Institute for Interdisciplinary Sciences, Tohoku University.

### Conflict of Interest

No potential conflicts of interest were disclosed.

### References

- Denaro AR, Hickling A. Glow-discharge electrolysis in aqueous solutions. *J Electrochem Soc* 1958; **105**: 265–270.
- Kanzaki Y, Hirabe M, Matsumoto O. Glow discharge electrolysis of aqueous sulfuric acid solution in various atmosphere. *J Electrochem Soc* 1986; **133**: 2267–2270.
- Kaneko T, Baba K, Hatakeyama R. Static gas-liquid interfacial direct current

- discharge plasmas using ionic liquid cathode. *J Appl Phys* 2009; **105**: 103306.
- 4 Richmonds C, Witzke M, Bartling B, *et al.* Electron-transfer reactions at the plasma-liquid interface. *J Am Chem Soc* 2011; **133**: 17582–17585.
  - 5 Tochikubo F, Shimokawa Y, Shirai N, Uchida S. Chemical reactions in liquid induced by atmospheric-pressure dc glow discharge in contact with liquid. *Jpn J Appl Phys* 2014; **53**: 126201.
  - 6 Baba K, Kaneko T, Hatakeyama R. Efficient synthesis of gold nanoparticles using ion irradiation in gas-liquid interfacial plasmas. *Appl Phys Exp* 2009; **2**: 035006.
  - 7 Shirai N, Uchida S, Tochikubo F. Synthesis of metal nanoparticles by dual plasma electrolysis using atmospheric dc glow discharge in contact with liquid. *Jpn J Appl Phys* 2014; **53**: 046202.
  - 8 Imasaka K, Suehiro J, Kanatake Y, Kato Y, Hara M. Preparation of water-soluble carbon nanotubes using a pulsed streamer discharge in water. *Nanotechnology* 2006; **17**: 3421–3427.
  - 9 Takeuchi N, Kitagawa Y, Kosugi A, Tachibana K, Obo H, Yasuoka K. Plasma-liquid interfacial reaction in decomposition of perfluoro surfactants. *J Phys D: Appl Phys* 2014; **47**: 045203.
  - 10 Fridman G, Friedman G, Gutsol A, Shekhter AB, Vasilets VN, Fridman A. Applied plasma medicine. *Plasma Process Polym* 2008; **5**: 503–533.
  - 11 Kong MG, Kroesen G, Morfill G, *et al.* Plasma medicine: an introductory review. *New J Phys* 2009; **11**: 115012.
  - 12 von Woedtke T, Reuter S, Masur K, Weltmann KD. Plasmas for medicine. *Phys Rep* 2013; **530**: 291–320.
  - 13 Park DP, Davis K, Gilani S, *et al.* Reactive nitrogen species produced in water by non-equilibrium plasma increase plant growth rate and nutritional yield. *Curr Appl Phys* 2013; **13**: S19–S29.
  - 14 Koga K, Sarinont T, Amano T, Shiratani M. Simple method of improving harvest by nonthermal air plasma irradiation of seeds of *Arabidopsis thaliana* (L.). *Appl Phys Exp* 2016; **9**: 016201.
  - 15 Sasaki S, Kanzaki M, Kaneko T. Calcium influx through TRP channels induced by short-lived reactive species in plasma-irradiated solution. *Sci Rep* 2016; **6**: 25728.
  - 16 Bruggeman P, Leys C. Non-thermal plasmas in and in contact with liquids. *J Phys D: Appl Phys* 2009; **42**: 053001.
  - 17 Sano N, Wang H, Chhowalla M, Alexandrou I, Amarantunga GAJ. Nanotechnology: synthesis of carbon ‘onions’ in water. *Nature* 2001; **414**: 506–507.
  - 18 Lisitsyn IV, Nomiya H, Katsuki S, Akiyama H. Streamer discharge reactor for water treatment by pulsed power. *Rev Sci Instrum* 1999; **70**: 3457–3462.
  - 19 Hieda J, Saito N, Takai O. Exotic shapes of gold nanoparticles synthesized using plasma in aqueous solution. *J Vac Sci Technol A* 2008; **26**: 854–856.
  - 20 Nomura S, Toyota H. Sonoplasma generated by a combination of ultrasonic waves and microwave irradiation. *Appl Phys Lett* 2003; **83**: 4503–4505.
  - 21 Ishijima T, Hotta H, Sugai H, Sato M. Multibubble plasma production and solvent decomposition in water by slot-excited microwave discharge. *Appl Phys Lett* 2007; **91**: 121501.
  - 22 Sato M, Ohgiyama T, Clements JS. Formation of chemical species and their effects on microorganisms using a pulsed high-voltage discharge in water. *IEEE Trans Ind Appl* 1996; **32**: 106–112.
  - 23 Ryzhkov VA. Carbon nanotube production by a cracking of liquid hydrocarbons. *Physica B* 2002; **323**: 324–326.
  - 24 Sano N, Nakano J, Kanki T. Synthesis of single-walled carbon nanotubes with nanohorns by arc in liquid nitrogen. *Carbon* 2004; **42**: 686–688.
  - 25 Tomai T, Katahira K, Kubo H, *et al.* Carbon materials syntheses using dielectric barrier discharge microplasma in supercritical carbon dioxide environments. *J Supercritical Fluids* 2007; **41**: 404–411.
  - 26 Bruggeman P, Brandenburg R. Atmospheric pressure discharge filaments and microplasmas: physics, chemistry and diagnostics. *J Phys D: Appl Phys* 2013; **46**: 464001.
  - 27 Winter J, Brandenburg R, Weltmann KD. Atmospheric pressure plasma jets: an overview of devices and new directions. *Plasma Sources Sci Technol* 2015; **24**: 064001.
  - 28 Keidar M. Plasma for cancer treatment. *Plasma Sources Sci Technol* 2015; **24**: 033001.
  - 29 Ahn HJ, Kim KI, Hoan NN, *et al.* Targeting cancer cells with reactive oxygen and nitrogen species generated by atmospheric-pressure air plasma. *Plos One* 2014; **9**: e86173.
  - 30 Iseki S, Nakamura K, Hayashi M, *et al.* Selective killing of ovarian cancer cells through induction of apoptosis by nonequilibrium atmospheric pressure plasma. *Appl Phys Lett* 2012; **100**: 113702.
  - 31 Fridman G, Peddinghaus M, Ayan H, Friedman G. Blood coagulation and living tissue sterilization by floating-electrode dielectric barrier discharge in air. *Plasma Chem Plasma Process* 2006; **26**: 425–442.
  - 32 Ikehara S, Sakakita H, Ishikawa K, *et al.* Plasma blood coagulation without involving the activation of platelets and coagulation factors. *Plasma Process Polym* 2015; **12**: 1348–1353.
  - 33 Arndt S, Unger P, Wacker E, *et al.* Cold atmospheric plasma (CAP) changes gene expression of key molecules of the wound healing machinery and improves wound healing *in vitro* and *in vivo*. *Plos One* 2013; **8**: e79325.
  - 34 Isbary G, Heinlin J, Shimizu T, *et al.* Successful and safe use of 2 min cold atmospheric argon plasma in chronic wounds: results of a randomized controlled trial. *Br J Dermatol* 2012; **167**: 404–410.
  - 35 Isbary G, Morfill G, Schmidt HU, *et al.* A first prospective randomized controlled trial to decrease bacterial load using cold atmospheric argon plasma on chronic wounds in patients. *Br J Dermatol* 2010; **163**: 78–82.
  - 36 Leduc M, Guay D, Leask RL, Coulombe S. Cell permeabilization using a non-thermal plasma. *New J Phys* 2009; **11**: 115021.
  - 37 Jinno M, Ikeda Y, Motomura H, Kido Y, Tachibana K, Satoh S. The necessity of radicals for gene transfection by discharge plasma irradiation. *J Photopolym Sci Technol* 2014; **27**: 399–404.
  - 38 Xu D, Wang B, Xu Y, *et al.* Intracellular ROS mediates gas plasma-facilitated cellular transfection in 2D and 3D cultures. *Sci Rep* 2016; **6**: 27872.
  - 39 Sasaki S, Kanzaki M, Kaneko T. Highly efficient and minimally invasive transfection using time-controlled irradiation of atmospheric-pressure plasma. *Appl Phys Exp* 2014; **7**: 026202.
  - 40 Kaneko T, Sasaki S, Hokari Y, Horiuchi S, Honda R, Kanzaki M. Improvement of cell membrane permeability using a cell-solution electrode for generating atmospheric-pressure plasma. *Biointerphases* 2015; **10**: 029521.
  - 41 Sasaki S, Honda R, Hokari Y, Takashima K, Kanzaki M, Kaneko T. Characterization of plasma-induced cell membrane permeabilization: focus on OH radical distribution. *J Phys D: Appl Phys* 2016; **49**: 334002.
  - 42 Sasaki S, Kanzaki M, Hokari Y, *et al.* Roles of charged particles and reactive species on cell membrane permeabilization induced by atmospheric-pressure plasma irradiation. *Jpn J Appl Phys* 2016; **55**: 07LG04.
  - 43 Graves DB. The emerging role of reactive oxygen and nitrogen species in redox biology and some implications for plasma applications to medicine and biology. *J Phys D: Appl Phys* 2012; **45**: 263001.
  - 44 Xu D, Liu D, Wang B, *et al.* *In situ* OH generation from O<sub>2</sub><sup>-</sup> and H<sub>2</sub>O<sub>2</sub>: plays a critical role in plasma-induced cell death. *Plos One* 2015; **10**: e0128205.
  - 45 Hofmann S, Sobota A, Bruggeman P. Transitions between and control of guided and branching streamers in DC nanosecond pulsed excited plasma jets. *IEEE Trans Plasma Sci* 2012; **40**: 2888–2899.
  - 46 Sobota A, Guitella O, Rousseau A. The influence of the geometry and electrical characteristics on the formation of the atmospheric pressure plasma jet. *Plasma Sources Sci Technol* 2014; **23**: 025016.
  - 47 Marinov D, Braithwaite NSJ. Power coupling and electrical characterization of a radio-frequency micro atmospheric pressure plasma jet. *Plasma Sources Sci Technol* 2014; **23**: 062005.
  - 48 van Gils CAJ, Hofmann S, Boekema BKHL, Brandenburg R, Bruggeman PJ. Mechanisms of bacterial inactivation in the liquid phase induced by a remote RF cold atmospheric pressure plasma jet. *J Phys D: Appl Phys* 2013; **46**: 175203.
  - 49 Bussiahn R, Gesche R, Kühn S, Weltmann KD. Integrated microwave atmospheric plasma source (IMAPLaS): thermal and spectroscopic properties and antimicrobial effect on *B. atrophaeus* spores. *Plasma Sources Sci Technol* 2012; **21**: 065011.
  - 50 Zaplotnik R, Bišćan M, Kregar Z, Cvelbar U, Mozetič M, Milošević S. Influence of a sample surface on single electrode atmospheric plasma jet parameters. *Spectrochim Acta B* 2015; **103**: 124–130.
  - 51 Kawasaki T, Kusumegi S, Kudo A, *et al.* Effects of irradiation distance on supply of reactive oxygen species to the bottom of a Petri dish filled with liquid by an atmospheric O<sub>2</sub>/He plasma jet. *J Appl Phys* 2016; **119**: 173301.
  - 52 Setsuhara Y, Uchida G, Kawabata K, Nakajima A, Takenaka K. Analysis of dynamic discharge characteristics of plasma jet based on voltage and current measurements using a metal plate. *IEEE Trans Plasma Sci* 2015; **43**: 3821–3826.
  - 53 Dobrynin D, Fridman A, Starikovskiy AY. Reactive oxygen and nitrogen species production and delivery into liquid media by microsecond thermal spark-discharge plasma jet. *IEEE Trans Plasma Sci* 2012; **40**: 2163–2171.
  - 54 Pipa AV, Reuter S, Foest R, Weltmann KD. Controlling the NO production of an atmospheric pressure plasma jet. *J Phys D: Appl Phys* 2012; **45**: 085201.
  - 55 Cruden BA, Rao MVVS, Sharma SP, Meyyappan M. Fourier-transform infrared and optical emission spectroscopy of CF<sub>4</sub>/O<sub>2</sub>/Ar mixtures in an

- inductively coupled plasma. *J Appl Phys* 2003; **93**: 5053–5062.
- 56 Fresnet F, Baravian G, Magne L, *et al.* Influence of water on NO removal by pulsed discharge in N<sub>2</sub>/H<sub>2</sub>O/NO mixtures. *Plasma Sources Sci Technol* 2002; **11**: 152–160.
  - 57 van Gessel AFH, Hrycak B, Jasiński M, Mizeraczyk J, van der Mullen JJAM, Bruggeman PJ. Temperature and NO density measurements by LIF and OES on an atmospheric pressure plasma jet. *J Phys D: Appl Phys* 2013; **46**: 095201.
  - 58 Verreycken T, van der Horst RM, Baede AHFM, van Veldhuizen EM, Bruggeman PJ. Time and spatially resolved LIF of OH in a plasma filament in atmospheric pressure He-H<sub>2</sub>O. *J Phys D: Appl Phys* 2012; **45**: 045205.
  - 59 Yonemori S, Ono R. Flux of OH and O radicals onto a surface by an atmospheric-pressure helium plasma jet measured by laser-induced fluorescence. *J Phys D: Appl Phys* 2014; **47**: 125401.
  - 60 Sakiyama Y, Graves DB, Chang H-W, Shimizu T, Morfill GE. Plasma chemistry model of surface microdischarge in humid air and dynamics of reactive neutral species. *J Phys D: Appl Phys* 2012; **45**: 425201.
  - 61 Traylor MJ, Pavlovich MJ, Karim S, *et al.* Long-term antibacterial efficacy of air plasma-activated water. *J Phys D: Appl Phys* 2011; **44**: 472001.
  - 62 Hänsch MAC, Mann M, Weltmann K-D, von Woedtke T. Analysis of antibacterial efficacy of plasma-treated sodium chloride solutions. *J Phys D: Appl Phys* 2015; **48**: 454001.
  - 63 Kanazawa S, Kawano H, Watanabe S, *et al.* Observation of OH radicals produced by pulsed discharges on the surface of a liquid. *Plasma Sources Sci Technol* 2011; **20**: 034010.
  - 64 Mason TJ, Lorimer JP, Bates DM, Zhao Y. Dosimetry in sonochemistry: the use of aqueous terephthalate ion as a fluorescence monitor. *Ultrason Sonochem* 1994; **1**: S91–S95.
  - 65 Kamibayashi M, Oowada S, Kameda H, *et al.* Synthesis and characterization of a practically better DEPMPO-type spin trap, 5-(2,2-dimethyl-1,3-propanoxy cyclophosphoryl)-5-methyl-1-pyrroline N-oxide (CYPMPO). *Free Radical Res* 2006; **40**: 1166–1172.
  - 66 Tani A, Ono Y, Fukui S, Ikawa S, Kitano K. Free radicals induced in aqueous solution by non-contact atmospheric-pressure cold plasma. *Appl Phys Lett* 2012; **100**: 254103.
  - 67 Tresp H, Hammer MU, Winter J, Weltmann KD, Reuter S. Quantitative detection of plasma-generated radicals in liquids by electron paramagnetic resonance spectroscopy. *J Phys D: Appl Phys* 2013; **46**: 435401.
  - 68 Kawasaki T, Kawano K, Mizoguchi H, *et al.* Visualization of the distribution of oxidizing substances in an atmospheric pressure plasma jet. *IEEE Trans Plasma Sci* 2014; **42**: 2482–2483.
  - 69 Kawasaki T, Sato A, Kusumegi S, *et al.* Two-dimensional concentration distribution of reactive oxygen species transported through a tissue phantom by atmospheric-pressure plasma-jet irradiation. *Appl Phys Exp* 2016; **9**: 076202.
  - 70 Jemal A, Bray F, Center MM, Ferlay J, Ward E, Forman D. Global Cancer Statistics. *Ca Cancer J Clin* 2011; **61**: 69–90.
  - 71 Niidome T, Huang L. Gene therapy progress and prospects: nonviral vectors. *Gene Ther* 2002; **9**: 1647–1652.
  - 72 Elbashir SM, Harborth J, Lendeckel W, Yalcin A, Weber K, Tuschl T. Duplexes of 21-nucleotide RNAs mediate RNA interference in cultured mammalian cells. *Nature* 2001; **411**: 494–498.
  - 73 Takahashi K, Yamanaka S. Induction of pluripotent stem cells from mouse embryonic and adult fibroblast cultures by defined factors. *Cell* 2006; **126**: 663–676.
  - 74 Neumann E, Schaefer-Ridder M, Wang Y, Hofschneider PH. Gene-transfer into mouse lymphoma cells by electroporation in high electric fields. *Embo J* 1982; **1**: 841–845.
  - 75 Bennink ML, Schärer OD, Kanaar R, *et al.* Single-molecule manipulation of double-stranded DNA using optical tweezers: interaction studies of DNA with RecA and YOYO-1. *Cytometry* 1999; **36**: 200–208.
  - 76 Rye HS, Yue S, Wemmer DE, *et al.* Stable fluorescent complexes of double-stranded DNA with bis-intercalating asymmetric cyanine dyes: properties and applications. *Nucleic Acids Res* 1992; **20**: 2803–2812.
  - 77 Norberg SA, Tian W, Johnsen E, Kushner MJ. Atmospheric pressure plasma jets interacting with liquid covered tissue: touching and not-touching the liquid. *J Phys D: Appl Phys* 2014; **47**: 475203.
  - 78 Tian W, Kushner MJ. Atmospheric pressure dielectric barrier discharges interacting with liquid covered tissue. *J Phys D: Appl Phys* 2014; **47**: 165201.
  - 79 Tian W, Kushner MJ. Long-term effects of multiply pulsed dielectric barrier discharges in air on thin water layers over tissue: stationary and random streamers. *J Phys D: Appl Phys* 2015; **48**: 494002.
  - 80 Takai E, Ikawa S, Kitano K, Kuwabara J, Shiraki K. Molecular mechanism of plasma sterilization in solution with the reduced pH method: importance of permeation of HOO radicals into the cell membrane. *J Phys D: Appl Phys* 2013; **46**: 295402.
  - 81 Wong-Ekkabut J, Xu Z, Triampo W, Tang IM, Tieleman DP, Monticelli L. Effect of lipid peroxidation on the properties of lipid bilayers: a molecular dynamics study. *Biophys J* 2007; **93**: 4225–4236.
  - 82 Joshi SG, Cooper M, Yost A, *et al.* Nonthermal dielectric-barrier discharge plasma-induced inactivation involves oxidative DNA damage and membrane lipid peroxidation in *Escherichia coli*. *Antimicrob Agents Chemother* 2011; **55**: 1053–1062.